



Advanced damper with high stiffness and high hysteresis damping based on negative structural stiffness

Liang Dong^{a,*}, Roderic Lakes^{b,c,*}

^aDepartment of Materials Science and Engineering, University of Virginia, Charlottesville, VA 22904, USA

^bMaterials Science Program, University of Wisconsin, Madison, WI 53706, USA

^cDepartment of Engineering Physics, University of Wisconsin, Madison, WI 53706, USA

ARTICLE INFO

Article history:

Received 19 July 2012

Received in revised form 8 March 2013

Available online 8 April 2013

Keywords:

Damping

Stiffness

Columns

Buckling

Uniaxial Compression

Experimental techniques

Structures

ABSTRACT

High structural damping combined with high stiffness is achieved by negative stiffness elements. Negative incremental structural stiffness occurs when a column with flat ends is subjected to snap-through buckling. Large hysteresis (i.e., high damping) can be achieved provided the ends of the column undergo tilting from flat to edge contact. The column configuration provides high structural stiffness. Stable axial dampers with initial modulus similar to that of the parent material and with enhanced damping were designed built and tested. Effective damping of approximately two and stiffness-damping product of approximately 200 GPa were achieved in such dampers consisting of stainless steel columns. This is a significant improvement for this figure of merit (i.e., the stiffness-damping product), which generally cannot exceed 0.6 GPa for currently used damping systems.

© 2013 Elsevier Ltd. All rights reserved.

1. Introduction

Mechanical damping is of vital importance as one can damp vibrations in mechanical systems so as to prolong the service life of components, also reduce acoustic noise. The measure of damping in linear systems is $\tan\delta$, with δ as the phase angle between stress and strain sinusoids. Damping of structures can be achieved via layers of high-damping materials, typically polymers, by external lumped dampers that may contain a viscous device, or using materials with intrinsically high damping. Structural metals such as steel, brass and aluminum alloys exhibit very low damping of 10^{-3} or less (steel: 0.0001; brass: 9×10^{-5} ; aluminum alloy: $<10^{-5}$) (Lakes, 2009). Material damping of structural metals is very low; therefore, structural damping obtained via specifically designed structures can be used in the cases where high damping is required to compensate for the drawback of low intrinsic damping. A maximal combination of stiffness and damping is desirable for the damping layer and structural damping applications in which it is intended that vibration in machinery and vehicles be reduced. In structures, this is the product of structural stiffness or spring constant and damping; in materials, it is the product $|E^*| \tan\delta$, with $|E^*|$ being the absolute value of the complex Young's modulus (E^*). Fig. 1 shows the stiffness-damping map for several

classes of material at ambient temperature. The diagonal line in Fig. 1 represents $|E^*| \tan\delta = 0.6$ GPa. Most materials occupy the region to the left of that line. Structural materials occupy regions to the left or far to the left in the diagram (i.e., high stiffness low damping). The $|E^*| \tan\delta$ product for structural metals are, for example, 0.02 GPa, 0.01 GPa and less than 0.001 GPa for steel, brass and aluminum alloy, respectively. Most rubbery materials occupy the lower right (i.e., low stiffness and high damping); the product $|E^*| \tan\delta$ is less than 0.003 GPa. Polymeric damping layers exhibit peak values in damping from 0.1 to 1 or more, therefore polymer layers are commonly used to add damping to structural members. However, the product $|E^*| \tan\delta$ generally does not exceed 0.6 GPa in such materials either; even this value can be attained only over a narrow range of temperatures near the glass transition region. In addition, damping layers work best for objects subjected to bending due to distance from the neutral axis; for axial deformation, they are not as effective. Therefore superior structures and materials are of interest. In particular, the region to the upper right of the diagonal line representing $|E^*| \tan\delta = 0.6$ GPa is favorable for vibration damping applications.

Materials and structures with high damping are intended for applications in which high damping is desired, for example to reduce vibration amplitude or to reduce the time scale for vibration to die out after an impulse. In the present study, negative stiffness was used to achieve high structural damping. Negative structural stiffness entails a reaction force in the same direction as the displacement. Such a condition is unstable unless it is constrained.

* Corresponding authors. Tel.: +1 608 346 7275 (L. Dong), +1 608 265 8697 (R. Lakes).

E-mail addresses: dongliang@uwalumni.com (L. Dong), lakes@engr.wisc.edu (R. Lakes).

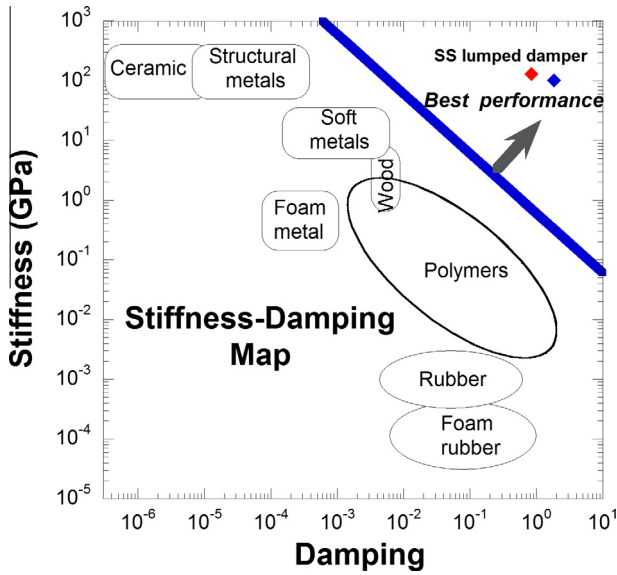


Fig. 1. Stiffness-damping map for several classes of materials in the linear regime at ambient temperature (adapted from Lakes, 2009). The diagonal line (i.e., the thick blue line) represents a constant figure of merit $|E^*|\tan\delta = 0.6 \text{ GPa}$. Commercial damping layers typically have a lower figure of merit. The solid diamond symbols represent the properties of the stainless steel damper modules in the nonlinear regime. (For interpretation of the references to color in this figure legend, the reader is referred to the web version of this article.)

For example a slender bar in a post-buckled ‘S’ shaped configuration is in unstable equilibrium (Bazant and Cedolin, 1991). If it is constrained laterally, it may be stabilized and the negative stiffness measured. Structures containing buckled tubes (Lakes, 2001a) exhibit negative stiffness that is observed under the constraint of displacement control. These structures exhibit extremely high structural damping under small oscillations when the pre-strain is appropriately tuned. The high damping is understood in the context of composite theory of Reuss (series) systems (Lakes, 2001a). Composite materials (Lakes, 2001b) (not structures) containing negative stiffness constituents are also predicted to exhibit extreme linear damping and anomalies in the stiffness. Such effects have been observed experimentally (Lakes et al., 2001; Jaglinski et al., 2007; Dong et al., 2011). Instability of a negative stiffness structure also gives rise to a nonlinear snap through effect that generates high effective damping. Structures based on lateral force on ‘S’ shaped beams or axial force on buckled flexible tubes provide a negative stiffness region (Lakes, 2001a) by which high structural damping can be attained via positive and negative stiffness in series (Lakes, 2001a). Follow-on efforts have further explored this concept (Kashdan et al., 2009, 2011; Haberman et al., 2012) but such structures are not very stiff. However, high stiffness is usually desired in structural applications. Therefore dampers were developed based on the negative stiffness of axially loaded columns with flat ends (Dong and Lakes, 2012). The design of the columns enables a snap-through buckling that gives rise to negative stiffness. The abrupt snap effect converts the low frequency input to a much higher frequency. Energy loss mechanisms are more effective at higher frequency. Indeed the damping ultimately converts the energy to thermal vibrations of atoms at frequencies greater than 10 GHz.

The ends are in a press fit condition and are free to tilt during buckling. A polymeric damper based on this concept was demonstrated (Dong and Lakes, 2012); stiffness comparable to that of the parent material was achieved, with greatly enhanced damping. In the present study a steel damper is developed with the aim of obtaining higher stiffness. In the present work, the post-buckling properties of flat ends press contact stainless steel (SS) columns

were experimentally studied; stable modules consisted of clamped and press contact SS columns were then constructed. The stiffness of the module is similar to that of the parent material but with greatly enhanced damping. Furthermore, it was found that with appropriate pre-strain and peak to peak displacement (denoted $u(P-P)$ in the figures), the effective damping of the damper module can attain values as high as approximately two, and a maximum stiffness-damping product of approximately 200 GPa was achieved, a significant improvement for this figure of merit.

2. Methods

Commercial SS (17-4PH, McMaster-Carr, tight-tolerance hardened) rods were used. SS columns of nominal 3.175 mm (1/8”) diameter with different lengths of 184, 150, and 125 mm were cut with a diamond saw and machined with a lathe to obtain a flat surface for both ends. Force displacement relationship measurements were performed at room temperature using a servohydraulic (maximum force capacity 100 kN, MTS system Corp. Mpls. MN) test system under compression in displacement control with 0.5 Hz sinusoidal waveforms as the input. A sufficient displacement enables post-buckling to occur during loading. The force and displacement waveforms were captured by a digital oscilloscope. Stable axial dampers were designed and built as proof of concept, taking advantage of the effects in post-buckling of press contact flat-ends columns. The frame of the damper module is composed of two 40 mm diameter 8 mm thick SS disk-shaped base plates supported by two identical dog-bone shaped SS rods clamped in between the two SS disk plates. The middle part of the dog-bone support rod is 92 mm in length and 3.175 mm in diameter; the two ends have effective length of 46 mm and diameter of 6.35 mm. The design of this module is shown in fig. 2. Engineering strain and stress were used in the present study.

Damping is inferred from load-deformation curves as follows. Damping ($\tan\delta$) is proportional to the area that is enclosed by the Lissajous figure (i.e., the closed curve of force vs. displacement sinusoidal). When the Lissajous figure is elliptic as it is in linear materials and structures, damping equals to the ratio of the width of the elliptic Lissajous figure to the length of the projection of this elliptic Lissajous figure onto the displacement axis. When the

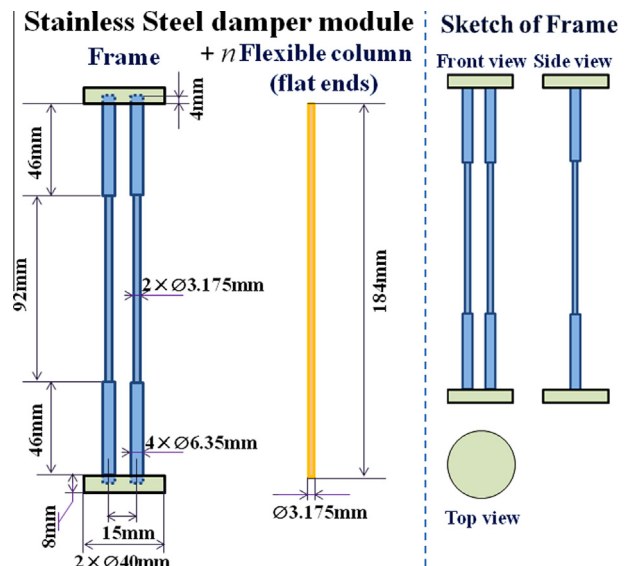


Fig. 2. Sketch of stainless steel axial damper module. The damper module is composed of a frame and one or more press contact flat ends columns (the quantity is represented by “n”). The frame is supported by two dog-bone support rods clamped in the disk-shaped base plates.

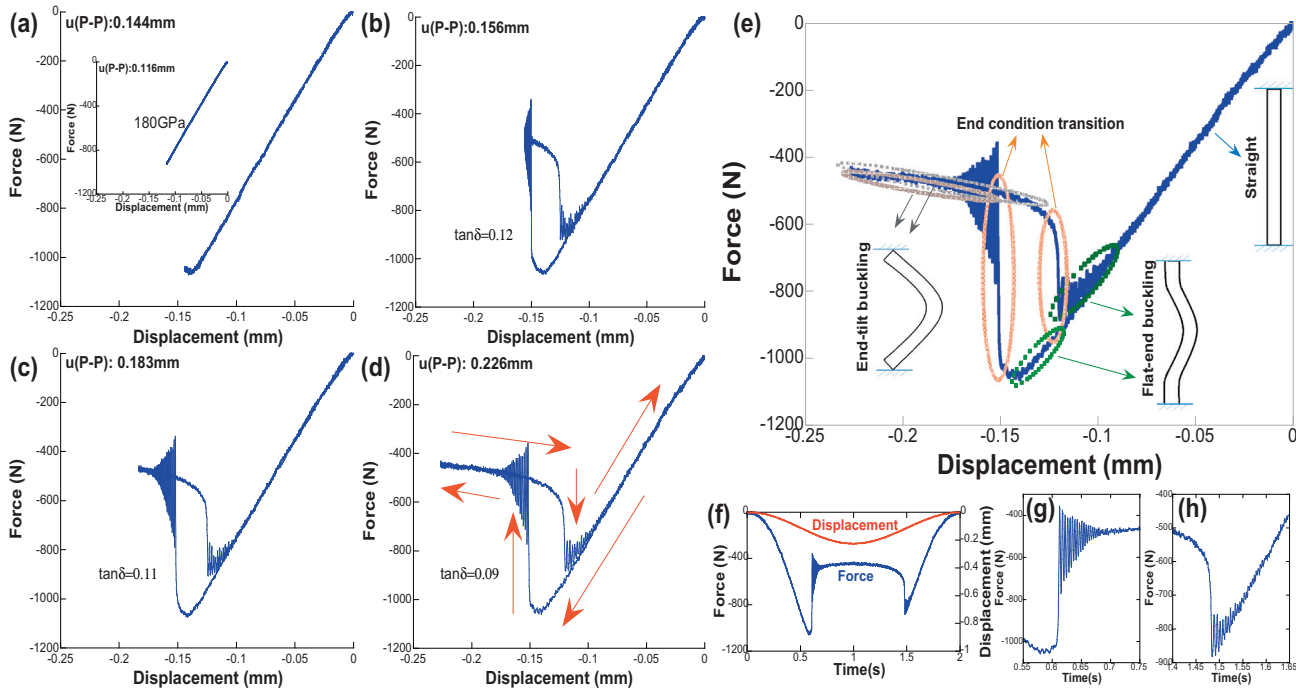


Fig. 3. (a)–(d) Force–displacement relationship of 3.175 mm diameter 184 mm length flat ends press contact stainless steel columns under 0.5 Hz compression tests at various displacements $u(P-P)$. Arrows in (d) show the path around loop. (e) Shows an example of a nonlinear Lissajous curve (the same as (d)) to illustrate how the end condition changes during loading history. Bending of columns in the line art figures is exaggerated. (f) Shows the displacement and force signals vs. time; (g) and (h) show the zoom-in of the force curve.

Lissajous figure exhibit nonlinearity, the shape is not elliptic; damping can be obtained by referring to the area ratio of this nonlinear Lissajous figure to an elliptic Lissajous figure with a known phase lag (e.g., $\delta = 1$ rad) within the same force–displacement rectangular boundaries (Lakes, 2009). The use of area entails the usual interpretation of damping in terms of energy loss. The interpreta-

tion of the hysteresis loops or Lissajous figures allows for the full nonlinearity of the system. The dissipation is calculated based on the area of the loop, hence the energy dissipated. If the system is nonlinear one refers to an effective $\tan\delta$. Results are presented in terms of an effective loss tangent to allow comparison with linear materials and systems. The specific damping capacity, usually denoted by a capital Greek Psi (Ψ), is the ratio of dissipated energy in one cycle divided by the stored energy in a quarter cycle. It is meaningful for both nonlinear systems and linear systems. In this study, to facilitate comparison with the efficacy of linear systems, the nonlinear damping derived from energy methods is expressed as the effective loss tangent, defined as the specific damping capacity, divided by 2π . The quantity Psi (Ψ) is meaningful for nonlinear materials as well as linear ones since the energies can be calculated from the stress–strain loop even if its shape is not elliptical. Since there are several possible ways of defining the stored energy, there are also several expressions for Psi (Nashif et al. (1985)). In the above, the stored elastic component of energy was used, in harmony with the results of Nashif et al. (1985). Quantitative interpretation of Lissajous figures can be found in (Lakes, 2009). For strong nonlinear system, e.g., the Lissajous curve shown in Fig. 3(b) which presents a “shovel” shape, the exact damping capacity cannot be extracted from the area enclosed by the hysteretic loop; the method employed in this paper can only estimate the approximate value of the damping capacity. To accurately calculate the damping capacity of a strong-nonlinear Lissajous figure requires more consideration and theoretical works.

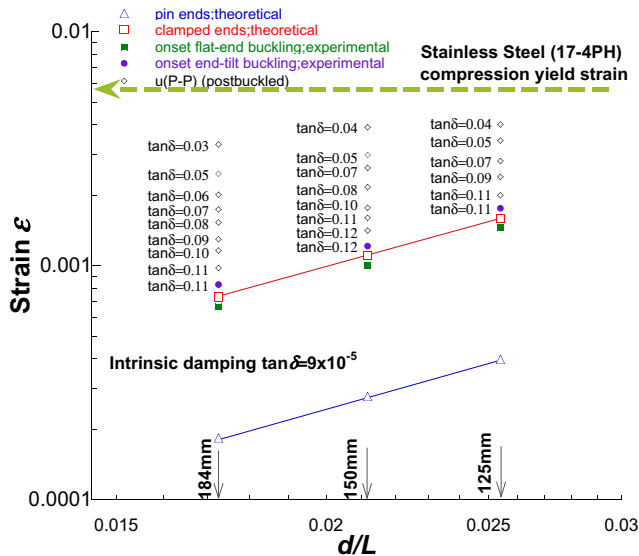


Fig. 4. Summary of flat ends stainless steel (17-4PH) column buckling: effective buckling strain vs. aspect ratio d/L . Critical effective strain of end contact tilting columns is between theoretical values for pin ends and clamped ends. Damping capacities at various peak to peak displacements $u(P-P)$ under compression (0.5 Hz) tests are summarized. Once buckling begins, damping greatly exceeds the intrinsic damping of the steel, less than 9×10^{-5} , too small to resolve by servo-hydraulic tests.

3. Results and discussion

Fig. 3 shows the force–displacement relationship of 3.175 mm diameter 184 mm length press contact column under 0.5 Hz compression tests at various peak to peak displacements $u(P-P)$. The inset of fig. 3(a) represents the linear viscoelastic behavior of SS column, and Young’s modulus is about 180GPa. Intrinsic damping

of SS is about 9×10^{-5} or less based upon resonant ultrasound spectroscopy (RUS) (Lee et al., 2000) measurement. With increasing amount of displacement $u(P-P)$, the end condition of the column changes from flat surface contact to edge contact, and the corresponding Lissajous figures exhibit nonlinearity as shown in Fig. 3(a)–(d). A negative slope, which indicates a negative stiffness on part of the force–displacement curve, is observed when the end condition changes due to tilt of the ends. The onset of end condition changing from flat surface contact to edge contact during the loading process is different from the onset of end condition changing from edge to flat surface contact during the unloading process. This difference entails a prominent hysteresis loop. The negative stiffness and the large hysteresis loop are attributed to the change of end conditions from flat to edge, which has been confirmed in our previous study (Dong and Lakes, 2012). Negative stiffness and the hysteresis loop attributed to contact change have also been reported by Estrin et al. (2003) and Schaare et al. (2008). Fig. 3(e) illustrates how the end condition changes during loading and unloading. Fig. 3(f) shows the force and displacement as a function of time, and (g) and (h) shows the zoomed in parts of the force vs. time. Energy dissipation occurs at the initial stage

when the end condition changes from one configuration to another. Snap through buckling gives rise to undulations in the force signal which diminish with time. Such undulations are relatively easy to damp since they are of high frequency. They can be minimized by utilizing high intrinsic damping materials (e.g., Zn alloy) or coating the SS column with a layer of material with high intrinsic damping which enhances energy attenuation. Such undulations in the force signal were not observed in the press contact PMMA columns during end condition transformation (Dong and Lakes, 2012); PMMA has a relatively high intrinsic damping of about 0.1.

Effective buckling strain vs. diameter to length ratio d/L of flat ends press contact SS (17-4PH) columns (without pre-strain) have been summarized in Fig. 4. The theoretical strains for losing stability of columns with pin ends and clamped ends according to Euler column buckling equations have been given as comparison with the experimental strains for the onset of buckling of flat ends press contact columns. The onset strain of flat-end buckling is determined as the strain at which the Lissajous figure starts to deviate from linearity. The Euler buckling equation (Hibbeler, 1991) is expressed as follows: $\varepsilon = \pi^2 I / [(KL)^2 A]$, where ε , I , K , L and A represent the theoretical strain for losing stability, area moment of inertia,

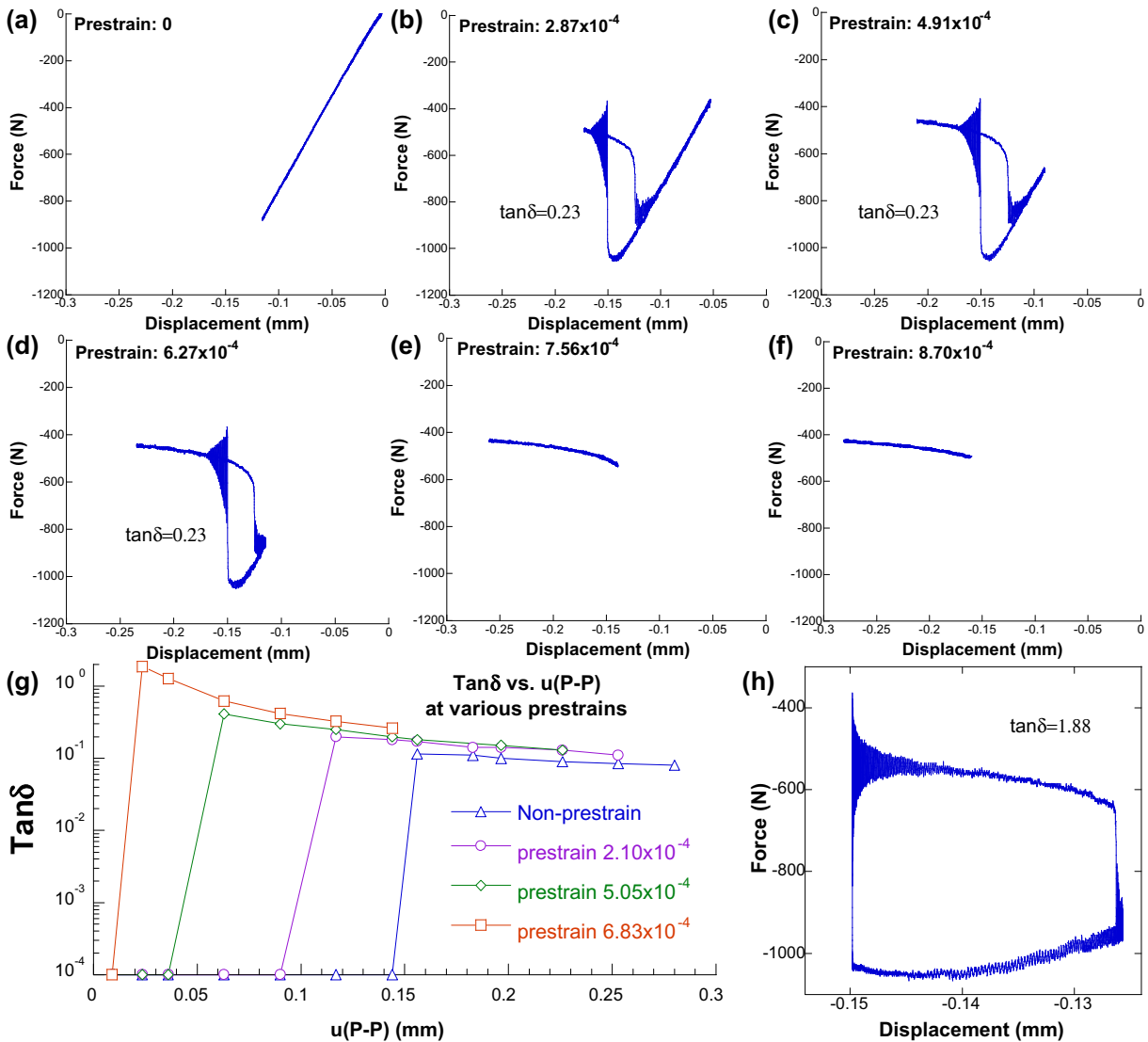


Fig. 5. (a)–(f) Force–displacement relationship of flat ends press contact 184 mm length 3.175 mm diameter stainless steel column as a function of pre-strain at fixed peak to peak displacement $u(P-P)$ (0.115 mm). (g) Summarizes the damping vs. peak-to-peak excursion in displacement at various pre-strains. (h) Shows the force–displacement hysteresis loop exhibiting with maximum attainable damping.

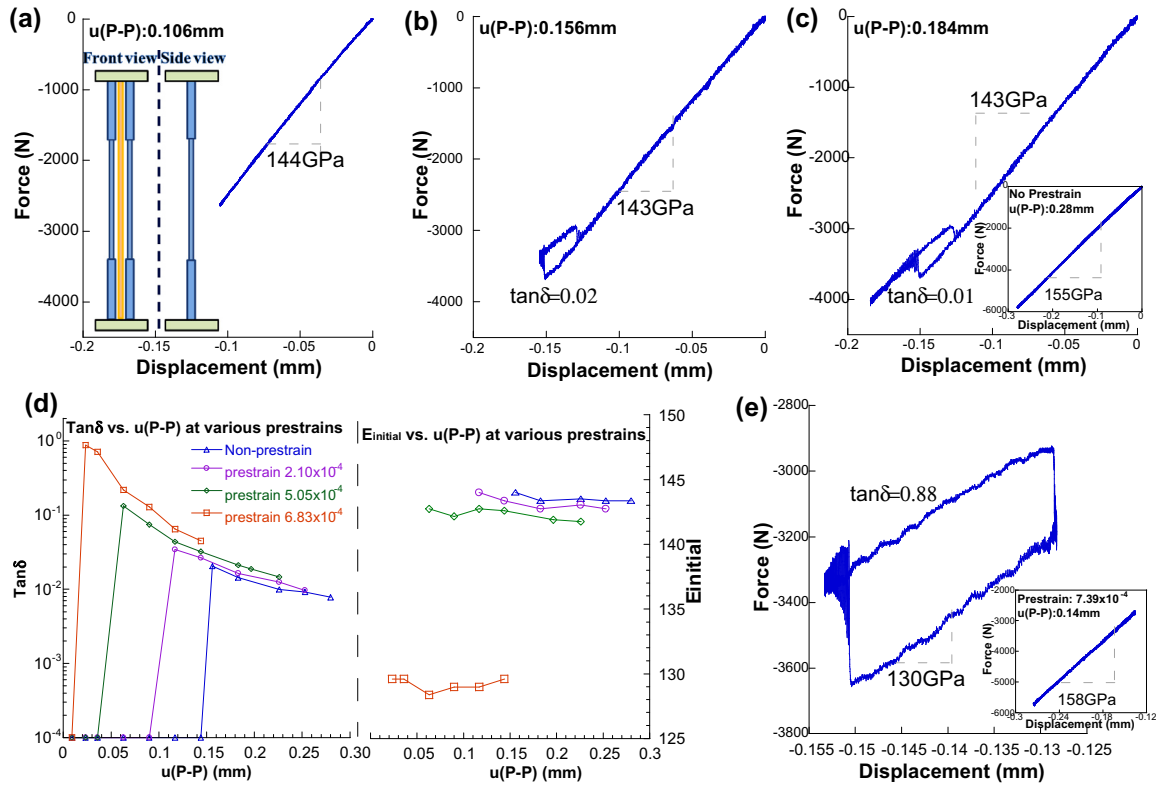


Fig. 6. (a)–(c) Force–displacement relationship of a non-pre-strained stainless steel axial damper module with one press contact flat ends stainless steel column ($L = 184$ mm; diameter = 3.175 mm) under 0.5 Hz compression tests at various peak to peak displacements $u(P-P)$. (d) Damping and initial stiffness of the module as a function of displacement $u(P-P)$. (e) Shows the force–displacement curve with maximum damping attained by this module. Insets in (a) show the sketch of this module. Curves show the force–displacement relationship of the non-pre-strained and pre-strained frame under 0.5 Hz compression tests.

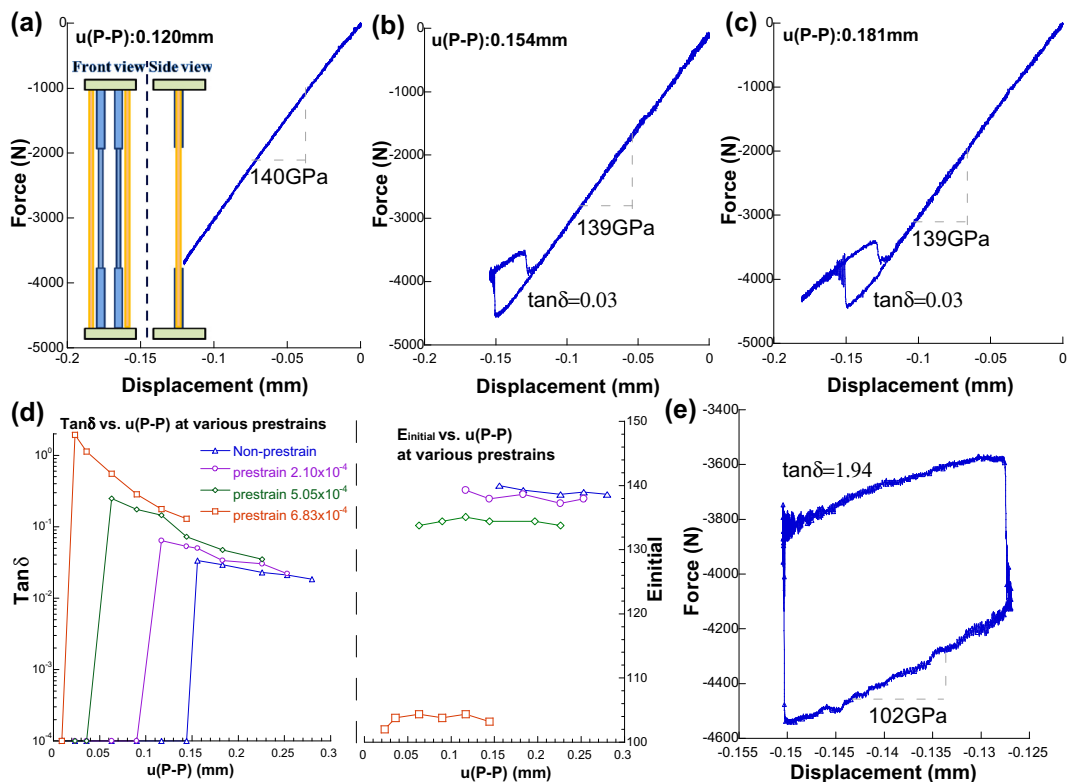


Fig. 7. (a)–(c) Force–displacement relationship of a non-pre-strained stainless steel axial damper module with two press contact flat ends stainless steel columns ($L = 184$ mm; diameter = 3.175 mm) under 0.5 Hz compression tests at various peak to peak displacements $u(P-P)$. (d) Damping and initial stiffness of the module as a function of peak to peak displacement $u(P-P)$. (e) Shows the force–displacement curve with maximum damping attained by this module with pre-strain. Insets in (a) show the sketch of this module.

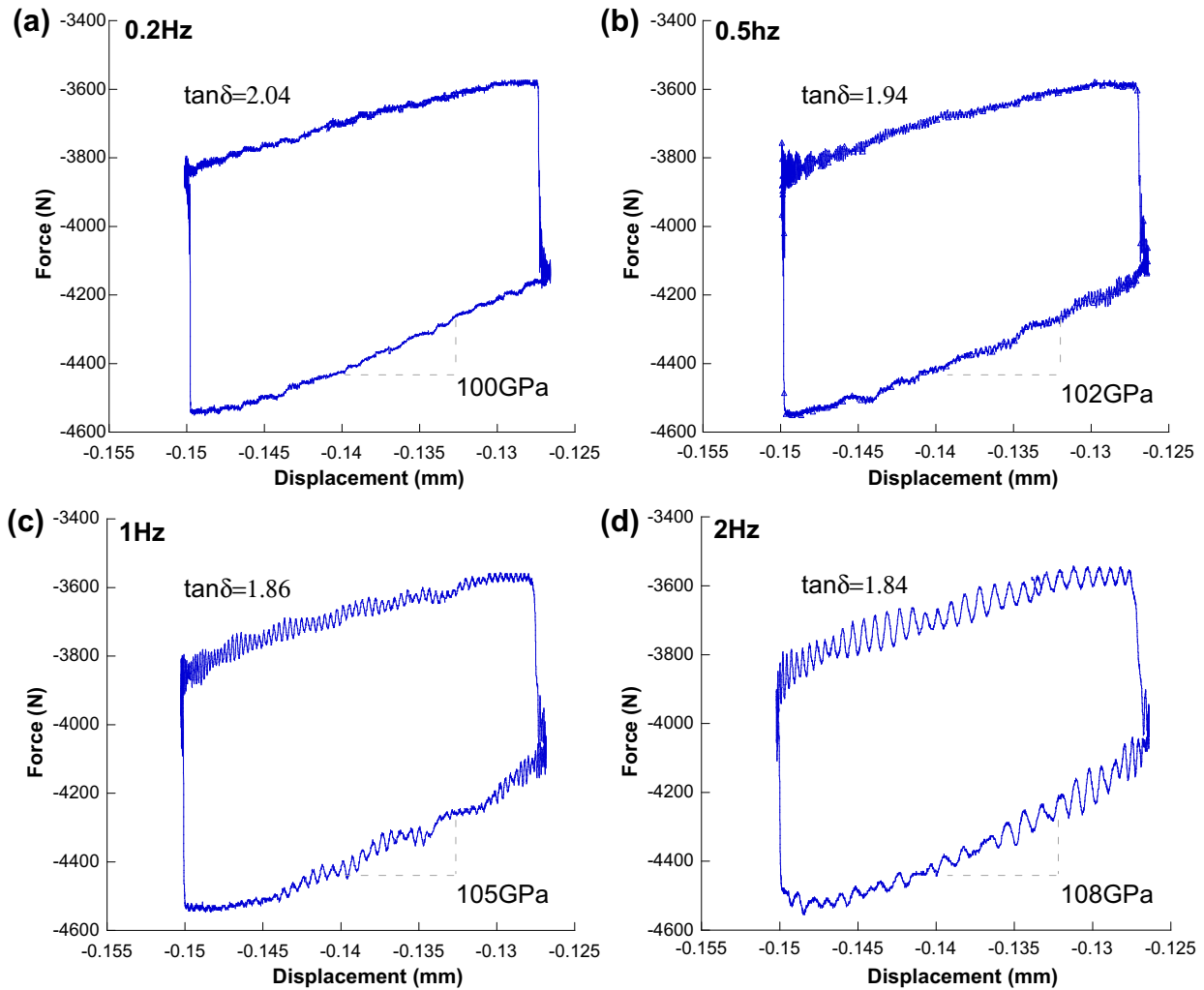


Fig. 8. Frequency dependence of the force–displacement relationship with maximum damping attained by the stainless steel axial damper module with two press contact flat ends stainless steel columns ($L = 184$ mm; diameter = 3.175 mm) under compression.

effective length factor, length of column, and cross-section area of the column, respectively. For columns with pin ends, $K = 1$; for columns with clamped ends, $K = 0.5$. Structural damping values at various peak-to-peak displacements ($u(P-P)$), for press-contact flat ends columns (without pre-strain) with different d/L ratios under 0.5 Hz compression have also been summarized in Fig. 4. By design, the columns are slender enough that during buckling, the compression yield strain of the steel (type 17-4PH SS) is never reached. The structural damping is dramatically higher than the intrinsic damping after the column has undergone end tilt buckling. Structural damping progressively decreases with increasing peak-to-peak displacement thereafter. d/L ratio has minimal effect on the structural damping of end tilted column. In this study, 184 mm length 3.175 mm diameter SS columns were used.

Damping is further increased if pre-strain is provided. Fig. 5 shows the properties of the 184 mm length 3.175 mm diameter flat ends press contact SS column as a function of pre-strain at fixed peak to peak displacement $u(P-P)$ (0.115 mm). A large hysteresis loop occurs and the linear portion of the Lissajous figure is reduced in length with increasing pre-strain. Following tuning of the pre-strain, only the segment corresponding to the post-buckling region (i.e., end-tilt buckling condition) remains. To get the maximum damping, it requires an appropriate pre-strain and a peak-to-peak excursion in displacement so that only the hysteresis loop remains on the force–displacement diagram. Fig. 5(h) shows the force–

displacement hysteresis loop exhibiting the maximum damping (about 1.88) that is attained by a press contact flat ends SS column ($L = 184$ mm; dia = 3.175 mm); the pre-strain is about 6.83×10^{-4} and displacement is about 0.024 mm. Damping as a function of displacement at various pre-strain levels has been summarized in Fig. 5(g). The end condition transition drastically increases the damping capacity by orders of magnitude from the intrinsic value (9×10^{-5} or less) at a fixed pre-strain; further increase in displacement gradually decreases the damping capacity as the post-buckling region grows.

The onset strain for losing stability of the middle part of the support rod of the module frame is about 0.003 according to the Euler column buckling equation; therefore the supporting portion of the module will be stable when the press contacting columns buckle as they are designed to do. The effective cross sectional area of the frame is calculated by referring to the Reuss composite model as follows, $A_{\text{frame}} = 2 / \{ [L_1 / (L_1 + 2L_2)] / A_1 + 2[L_2 / (L_1 + 2L_2)] / A_2 \}$, where L_1 , A_1 and L_2 , A_2 represent the length and the cross sectional area of the 3.175 mm diameter rod and 6.35 mm diameter rod, respectively. The bases of the module frame are not considered in calculation in that they are very stiff due to their large area, similarly to the compression plates of the servohydraulic machine. When press-fit flat ends SS columns are incorporated, the effective cross sectional area of the damper module is expressed as $A_{\text{effective}} = A_{\text{frame}} + nA_{\text{column}}$, where n and A_{column} represent the

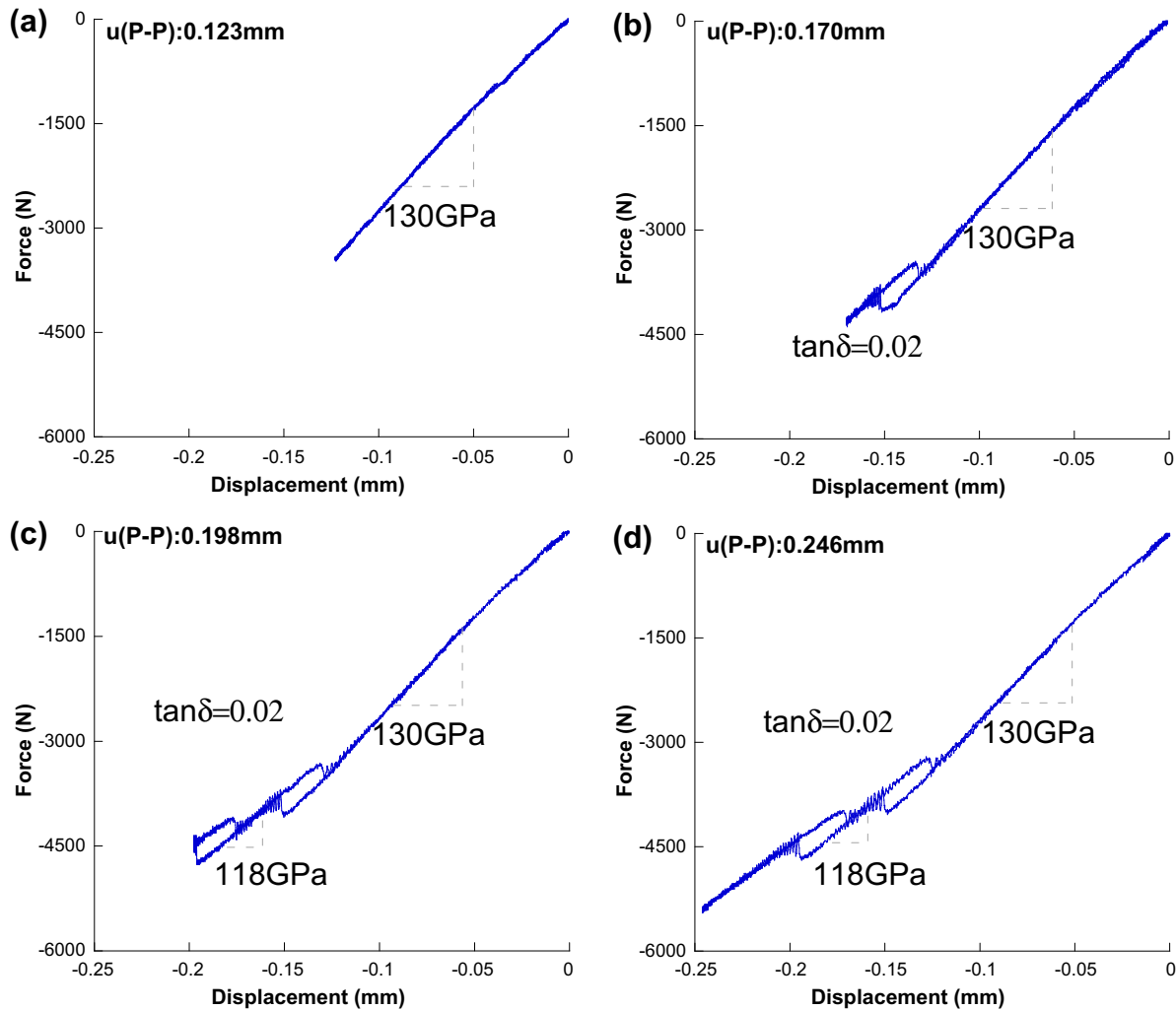


Fig. 9. Force–displacement relationship of a non-pre-strained stainless steel axial damper module with two press contact flat ends stainless steel columns ($L = 184$ mm; diameter = 3.175 mm) with slight length difference ($\Delta L \approx 0.044$ mm) under 0.5 Hz compression tests at various peak to peak displacements $u(P-P)$.

number of press-fit columns being used and the cross sectional area of such a column.

Fig. 6(a)–(c) presents the behaviors of the damper module with one press contact 3.175 mm diameter 184 mm length flat ends SS column under 0.5 Hz compression tests without pre-strain. With increasing displacement $u(P-P)$, damping capacity of the module increases by virtue of the end condition transition of the press contact column, and the squared-off shape of the Lissajous figure is an indication of the press contact column buckling. The effective stiffness of the module is similar to that of the parent material. The seating effect due to initial contact during this type of compression measurement lowers the apparent initial stiffness of the module. This reduction could be ameliorated by refinements in the machining of the contact surfaces. Damping and initial stiffness of this damper module as a function of displacement at various pre-strain levels have been summarized in Fig. 6(d). The initial stiffness is the stiffness at the small strain loading stage determined by the slope of the tangent line of the initial loading portion. Appropriate pre-strain ($\sim 6.84 \times 10^{-4}$) and peak to peak displacement (~ 0.022 mm) allow the force–displacement hysteresis loop to remain corresponding to a maximum damping of about 0.88 attainable by such a damper module; the corresponding initial stiffness of the module is about 130 GPa. Therefore, a maximum stiffness–damping product ($|E^*| \tan \delta$) of about 114 GPa is achieved in such a damper module. The behaviors of the module are in the nonlinear

range of viscoelasticity, as shown by the fact the hysteresis loops are not elliptic.

Damping capacity of the damper module is further increased with additional press contact flat ends columns. Fig. 7 presents the behaviors of the module with two press contact flat ends columns under 0.5 Hz compression tests. (a)–(c) shows the behaviors of this module with no pre-strain, and (d) summarizes the damping and initial stiffness of this module as a function of displacement at various pre-strain levels. Appropriate pre-strain ($\sim 6.87 \times 10^{-4}$) and displacement (~ 0.023 mm) give rise to a maximum damping of about 1.94. The corresponding initial stiffness of the module is about 102 GPa. Again, this is lower than that of steel due to imperfect contact conditions. Therefore, a maximum stiffness–damping product ($|E^*| \tan \delta$) of about 198 GPa is achieved by the damper module with two press contact flat ends columns. The maximum damping achieved by this module is higher than the maximum damping attained by a single press contact column. This is not surprising because the undulations on the force signal of the press contact columns are averaged out by the frame which allows the Lissajous figure to occupy more area within the same force–displacement rectangular boundaries, which gives rise to a higher damping capacity. As for the frequency dependence, Fig. 8 shows the responses corresponding to the maximum damping capacity that can be attained by this module (with two identical press contact flat ends columns) at various frequencies (0.2, 0.5,

1, and 2 Hz). Frequency dependence over the frequencies accessible is minimal. Higher frequency was not used as it approaches the resonance of the instrument.

As for non-ideal behavior, effective stiffness was in some tests lower than that of the steel, due to imperfect contact conditions. This can be ameliorated by refinements in machining of the surfaces. Moreover, plastic indentation at the edges in contact with the base due to stress concentration was observed, and this becomes more severe when the column length becomes shorter. This can give rise to a change in the buckling threshold but does not reduce or abolish the hysteresis damping.

The damper module, in contrast to polymer damping materials, is nonlinear, so it is appropriate for use to damp relatively large amplitudes of shock or vibration. A module based on steel or other structural metal is also insensitive to temperature. By contrast, polymer damping materials typically perform well over a restricted temperature range of 10–20 °C because they are based on the high damping that occurs near the glass–rubber transition.

In summary, the SS damper module occupies the upper right region of the stiffness–damping map, and the maximum stiffness–damping product ($|E^*|\tan\delta$) greatly exceeds 0.6 GPa. Negative incremental structural stiffness and large hysteresis (i.e., high damping) is achieved when the end condition of a press contact flat ends column changes from flat surface to edge contact. With appropriate pre-strain and displacement, damping higher than one is achieved. Such an idea can be used to design stable axial damper module with stiffness similar to that of the parent material but with enhanced damping capacity. The pre-strain can be provided by a shim or a screw system. Addition of more damper columns can also increase the overall damping.

To make such damper modules to be more effective so that they can function at various strain levels, one can use press contact columns with different diameter to length ratios; flat surface to edge contact transition would occur progressively as the strain increases. Fig. 9 gives an example of hysteresis at 0.5 Hz of a non-pre-strained damper module with two press contact flat ends stainless steel columns ($L = 184$ mm; diameter = 3.175 mm) with a slight length difference ($\Delta L \approx 0.044$ mm). Various peak to peak displacements $u(P-P)$ were applied. The double loop pattern arises because each column has a slightly different buckling threshold (the threshold is attributed to the contact condition). Such a damper module can operate over a wider range of strain than modules based on columns with a single aspect ratio d/L . A similar effect could be obtained by using columns of the same length but different diameter.

As for how are these high damping level values obtained in the experiment will be affected by the mass and stiffness properties of the overall structure, it is considered that if mass and stiffness of the overall structure are such that the frequency spectrum is within the range reported here, it is expected that the results will be useful for the design of dampers; if not, further experiments are called for to broaden the range.

4. Conclusion

Negative stiffness and large hysteresis damping can be achieved when a column with flat ends is subjected to snap-through buckling. With appropriate pre-strain, the damping capacity of such a column can be tuned to exceed one. Stable axial damper modules composed of clamped and press contact flat ends SS columns have designed and tested. A maximum effective damping of two and a stiffness–damping product of about 200 GPa has been achieved in such a pre-strained damper module. This represents a large improvement for this figure of merit which generally cannot exceed 0.6 GPa for currently used damping systems.

Acknowledgment

Support from DARPA is gratefully acknowledged.

References

- Bazant, Z., Cedolin, L., 1991. *Stability of Structures*. Oxford University Press, Oxford.
- Dong, L., Lakes, R.S., 2012. Advanced damper system with negative structure stiffness elements. *Smart Mater. Struct.* 21, 075026.
- Dong, L., Stone, D.S., Lakes, R.S., 2011. Extreme an elastic responses in $Zn_{80}Al_{20}$ matrix composite materials containing $BaTiO_3$ inclusion. *Scripta Mater.* 65, 288–291.
- Estrin, Y., Dyskin, A.V., Pasternak, E., Schaare, S., Stanchits, S., Kanel-Belov, A.J., 2003. Negative stiffness of a layer with topologically interlocked elements. *Scripta Mater.* 50, 291–294.
- Haberman, M., Klatt, T.D., Wilson, P.S., Seepersad, C.C., 2012. Negative stiffness metamaterials and periodic composites. *J. Acoust. Soc. Am.* 131, 3372.
- Hibbeler, R.C., 1991. *Mechanics of Materials*. Macmillan Publishing Company, New York.
- Jagliniski, T., Stone, D.S., Kochmann, D., Lakes, R.S., 2007. Materials with viscoelastic stiffness greater than diamond. *Science* 315, 620–622.
- Kashdan, L., Haberman, M., Wilson, P.S., Seepersad, C.C., 2009. Negative stiffness metamaterial elements for enhanced material damping capacity. *J. Acoust. Soc. Am.* 126, 2280.
- Kashdan, L., Seepersad, C.C., Haberman, M., Wilson, P.S., 2011. Design, fabrication, and evaluation of negative stiffness elements using SLS. *Rapid Prototyping J.* 18, 194–200.
- Lakes, R.S., 2001a. Extreme damping in compliant composites with a negative stiffness phase. *Philos. Mag. Lett.* 81, 95–100.
- Lakes, R.S., 2001b. Extreme damping in composite materials with a negative stiffness phase. *Phys. Rev. Lett.* 86, 2897–2900.
- Lakes, R.S., 2009. *Viscoelastic Materials*. Cambridge University Press.
- Lakes, R.S., Lee, T., Bersie, A., Wang, Y.C., 2001. Extreme damping in composite materials with negative stiffness inclusions. *Nature* 410, 565–567.
- Lee, T., Lakes, R.S., Lal, A., 2000. Resonant ultrasound spectroscopy for measurement of mechanical damping: comparison with broadband viscoelastic spectroscopy. *Rev. Sci. Instrum.* 71, 2855–2861.
- Nashif, A.D., Jones, D.I.G., Henderson, J.P., 1985. *Vibration Damping*. J. Wiley, NY.
- Graesser, E. J. and Wong, C. R., 1992. The relationship of traditional damping measures for materials with high damping capacity: a review, in M3D: Mechanics and Mechanisms of Material Damping, In: V. K. Kinra, A. Wolfenden, (Ed.), ASTM 1916 Race St. Phila. PA, Volume ASTM STP 1169.
- Schaare, S., Dyskin, A.V., Estrin, Y., Arndt, S., Pasternak, E., Kanel-Belov, A., 2008. Point loading of assemblies of interlocked cube-shaped elements. *Int. J. Eng. Sci.* 46, 1228–1238.